A&A 458, 625–633 (2006)
DOI: 10.1051/0004-6361:20054591

Astronomy & Astrophysics

Collisional influence on the differential Hanle effect method applied to the second solar spectrum of the $A^2\Pi$–$X^2\Sigma^+$ (0, 0) band of MgH⋆

V. Bommier[1], E. Landi Degl'Innocenti[2], N. Feautrier[1], and G. Molodij[3]

[1] Laboratoire d'Étude du Rayonnement et de la Matière en Astrophysique, CNRS UMR 8112 – LERMA, Observatoire de Paris, Section de Meudon, 92195 Meudon, France
e-mail: V.Bommier@obspm.fr
[2] Università degli Studi di Firenze, Dipartimento di Astronomia e Scienza dello Spazio, Largo E. Fermi 2, 50125 Firenze, Italy
[3] Laboratoire d'Études Spatiales et d'Instrumentation en Astrophysique, CNRS UMR 8109 – LESIA, Observatoire de Paris, Section de Meudon, 92195 Meudon, France

Received 25 November 2005 / Accepted 28 July 2006

ABSTRACT

Aims. This paper presents an analysis of the $Q_{1,2}(6-12)$ lines of the Q band of the $A^2\Pi$–$X^2\Sigma^+$ (0, 0) transition of MgH, whose linear polarization was measured 4 arcsec inside the solar limb in a quiet region (North Pole) with THEMIS on 21 November 2004.
Methods. This analysis is performed as follows: a) the Hanle effect Γ_H parameter is derived by applying the differential Hanle effect method between the two extreme pairs of lines. Assuming no depolarizing collisions, a magnetic field strength follows, which is found to be 9.2 Gauss, in agreement with previous observations of the same kind; b) this Γ_H parameter is entered in a code solving the NLTE polarized radiative transfer equations, and the other depolarizing parameter, namely the depolarizing collision rate, is then derived by adjusting the computed polarization to the observed one. Thus an average value of the rate per colliding hydrogen atom $\alpha^{(2)} = 1.20 \times 10^{-9}$ cm^3 s^{-1} is obtained for the upper levels of the 12 lines (standard deviation 0.21×10^{-9} cm^3 s^{-1}). The corresponding model-dependent depolarizing rate is $D^{(2)} = (4.2 \pm 0.7) \times 10^7$ s^{-1} at $h = 200$ km; c) this depolarizing rate is now introduced in the conversion of the Γ_H parameter in terms of magnetic field strength: an average turbulent field strength of 29 ± 12 Gauss is derived as the final value, at height $h = 200 \pm 80$ km where the polarization is formed. The Hönl-London factors of the lines under interest have been recalculated, leading to detect an error of a factor 2 in the recent literature.
Results. The derived value $B = 29 \pm 12$ Gauss at $h = 200 \pm 80$ km is in fairly good agreement with the previous determinations based on the interpretation of the Sr I 4607 Å limb polarization, which has led to fields in the range 35–60 Gauss.
Conclusions. Given the error bars, it seems unnecessary to put forward different formation regions for the Sr I and MgH lines.

Key words. Sun: magnetic fields – polarization

1. Introduction

Since the first observations of molecular lines in the "second solar spectrum" (the linear polarization spectrum near the Quiet Sun limb) by Stenflo & Keller (1997), Gandorfer's atlas of the second solar spectrum (Gandorfer 2000) has revealed their richness, and in particular that the wavelength region 5170–5182 Å displays a series of MgH lines, the $Q_{1,2}(6-12)$ lines of the Q band of the $A^2\Pi$–$X^2\Sigma^+$ (0, 0) transition (as identified by Berdyugina et al. 2002), that are free of any blend, so that we have undertaken a scan of this second solar spectrum portion with THEMIS on 26 October 2001. A second scan has been performed on 21 November 2004.

A preliminary common knowledge was that the second solar spectrum molecular lines would be "immune to the Hanle effect" (see the first interpretation by Berdyugina et al. 2002), but a theoretical investigation by Landi Degl'Innocenti (2003) pointed out that, even if their Landé factors are smaller than the atomic ones, their level inverse lifetimes are also smaller in the same range, so that a sensitivity to the Hanle effect analogous to the one of atomic lines can be expected. Moreover, molecular lines are particularly suitable for applying a method of multi-line determination of the magnetic field, given the fact that in a band the Landé factor may vary by more than a factor 2 for a given branch and even by an order of magnitude when comparing different branches. The multi-line or differential method for diagnosing solar magnetic fields through the Hanle effect was pioneered by Bommier et al. (1981) and by Landi Degl'Innocenti (1982) who took advantage of the different Hanle sensitivity of the two components of the D_3 line of He I to diagnose magnetic fields in solar prominences. For molecular lines, first interpretative works recently appeared, taking advantage of the differential Hanle effect method, as reviewed in details by Berdyugina & Fluri (2004), who apply it to two well resolved C_2 line triplets. Their observation data were taken from Gandorfer's atlas (Gandorfer 2000). Other less resolved C_2 triplets, taken from the same atlas, have been investigated by Trujillo Bueno (2003a,b), and their conclusions in favor of a weak field can be found in Trujillo Bueno et al. (2004). Faurobert & Arnaud (2002, 2003) develop a line formation model, based on the fact that most molecular lines of the second solar spectrum have no visible counterpart in the intensity spectrum (the "first spectrum"). Thus, these molecular lines are optically thin, so that modelling their formation results in two steps: a) modelling the anisotropy

⋆ Based on observations made with the French-Italian telescope THEMIS operated by the CNRS and CNR on the island of Tenerife in the Spanish Observatorio del Teide of the Instituto de Astrofísica de Canarias.

of the incident continuum; b) integrating their scattered polarization along the line-of-sight. They apply their model to the interpretation of MgH and C_2 lines observed with THEMIS. Taking into account a remaining error of a factor of 2, all the above athors agree now on a value of 7 Gauss for the magnetic field strength ("Polarized Solar Molecules" Workshop, Meudon (France), 17 December 2004, V. Bommier org.). However, the depolarizing effect of collisions was excluded from all these analyses, because the rate are fully unknown.

Nevertheless, the magnetic field determination from the Hanle effect observed in the Sr I 4607 Å line has led to field strengths in the range 35–60 Gauss (Faurobert et al. 2001; Trujillo Bueno et al. 2004; Bommier et al. 2005). As the two ranges of field strength are found different, Trujillo Bueno et al. (2004) conclude to different line formation regions for C_2 and Sr I.

The aim of the present work is to investigate the depolarizing collision effect on the magnetic field strength determination, by simultaneously deriving both quantities from our data. This will be achieved as follows:

– first, the differential Hanle effect method is applied to the two extreme pairs of lines. Farther are the lines one from each other, moresensitive is their ratio. This leads to the determination of the Hanle parameter $\Gamma_{\rm H}$, that determines the Hanle depolarization parameter $W_{\rm H}$ (see Eq. (25) below). At this stage, the derivation of the magnetic field strength requires the knowledge of the collisional depolarizing rate, because both contribute to $\Gamma_{\rm H}$;
– second, a model of NLTE polarized radiative transfer is run, where the Hanle parameter $\Gamma_{\rm H}$ previously determined is introduced, and the depolarizing collision rate that is let free is determined by comparing the computed and observed polarizations;
– third, the depolarizing rate thus determined is applied to the field strength derivation from $\Gamma_{\rm H}$.

As detailed in Sect. 4, such a reasoning applies to lines having not too different quantum numbers and formation mechanisms, as the present ones that belong to the same band. The observations are described in Sect. 2, the three steps of the interpretation are described in Sect. 4, and the conclusion is drawn in Sect. 5. Section 3 is devoted to the recalculation of the Hönl-London factors of the lines under interest.

2. Observations

Two observations have been obtained with THEMIS: 26 October 2001 and 21 November 2004. This telescope has the original feature of being "polarization free", i.e. the polarization analysis is performed on axis, before any oblique reflection. The second original feature of THEMIS is the one of being able to simultaneously record several spectral windows, in order to probe the solar atmosphere along depth, because the different lines simultaneously observed are formed at different altitudes. A more detailed description of the THEMIS instrument can be found in Arnaud et al. (1998), though it has to be updated as regards the tip-tilt correction, which has been modified and is not yet (but nearly) operational at the moment where these words are written, and the polarization analyzer quarter-wave plate positions that are now free to take any position needed.

These observations have been achieved following the method described in Bommier & Molodij (2002). The slit was

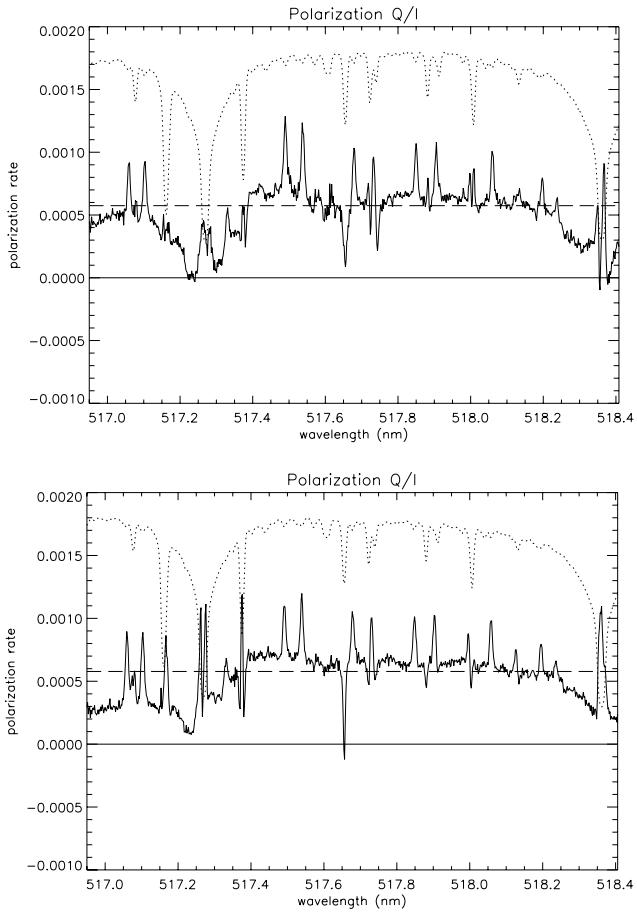

Fig. 1. Spectrum of the linear polarization along the limb Q/I observed 4 arcsec inside the North Pole limb on 26 October 2001 (*top*) and 21 November 2004 (*bottom*) with THEMIS. The data have been averaged along the slit, which was 120 arsec long and positioned parallel to the limb. The polarization peaks are those of the $Q_{1,2}(6-12)$ lines of the Q band of the $A^2\Pi-X^2\Sigma^+$ (0, 0) transition of MgH. Dotted line: intensity spectrum (arbitrary units except the zero line).

positioned parallel to the limb, in a quiet region (North Pole). To increase the polarimetric sensitivity, the data have been averaged along the slit, removing thus any spatial resolution. Limb and flat-field slices of images have been interleaved (3 slices of 10×6 images), to ensure a proper fringe elimination by using the flat-field images. The analysis technique is the one of Bommier & Molodij (2002), using the basic bricks of Bommier & Rayrole (2002), except from the fact that now any position is allowed for the quater waveplates of the polarization analyser, so that the beam exchange has been separately performed in every polarization Stokes parameter Q, U, V, leading to six waveplate different positions for each single image. The observation was one day long each time, and five different spectral windows were recorded and then assembled.

The result is given in Fig. 1, upper part being the 2001 data and lower part being the 2004 data. The regularly spaced polarization peaks that appear in both figures are due to the $Q_{1,2}(6–12)$ lines of the Q band of the $A^2\Pi–X^2\Sigma^+$ (0, 0) MgH transition, whose wavelengths are given in Table 1. The $Q_{1,2}(11)$ pair of lines, that would fall exactly inside one of these two lines, is not visible. We think that the polarization peaks that appear in the core of the two deep Mg I b lines and other deep lines that are visible in the figure, are artefacts due to the low intensity level in these line cores. As these peaks are different in

Table 1. Physical data for the observed lines. The excitation potential is that of the lower level ℓ. The Landé factor is that of the upper level u. The wavelengths are taken from Schadee (1964), and the oscillator strengths have been derived from the gf values provided in the Kurucz's data base. As for the line polarizability W_2, see text.

(N_ℓ)	Wavelength Å	Oscillator strength	$A_{u\ell}$ s^{-1}	Excitation potential (eV)	Landé factor	W_2
$Q_1(6)$	5181.930	0.0789	1.95880E+07	0.029864	0.17582	0.38681
$Q_1(7)$	5180.593	0.0792	1.96892E+07	0.039819	0.15000	0.39000
$Q_1(8)$	5179.032	0.0796	1.97850E+07	0.051196	0.13072	0.39216
$Q_1(9)$	5177.293	0.0798	1.98549E+07	0.063995	0.11579	0.39368
$Q_1(10)$	5175.419	0.0799	1.98974E+07	0.078216	0.10390	0.39481
$Q_1(11)$	5173.325	0.0801	1.99692E+07	0.093859	0.09420	0.39565
$Q_1(12)$	5171.012	0.0802	1.99977E+07	0.110925	0.08615	0.39631
$Q_2(6)$	5181.307	0.0780	1.93665E+07	0.029864	-0.12821	0.38462
$Q_2(7)$	5179.994	0.0787	1.95579E+07	0.039819	-0.11429	0.38857
$Q_2(8)$	5178.503	0.0792	1.97052E+07	0.051196	-0.10294	0.39118
$Q_2(9)$	5176.816	0.0794	1.97566E+07	0.063995	-0.09357	0.39298
$Q_2(10)$	5174.895	0.0796	1.98276E+07	0.078216	-0.08571	0.39429
$Q_2(11)$	5172.806	0.0799	1.99170E+07	0.093859	-0.07905	0.39526
$Q_2(12)$	5170.574	0.0799	1.99441E+07	0.110925	-0.07333	0.39600

Table 2. Linear polarization degree (above the continuum) observed in the lines of the Q band of the $A^2\Pi$–$X^2\Sigma^+$ (0, 0) transition of MgH, on 26 October 2001 and 21 November 2004 with THEMIS, and the one recorded in the Second Solar Spectrum Atlas by Gandorfer (2000).

(N_ℓ)	THEMIS 2001	THEMIS 2004	Atlas 1999-2000
$Q_1(6)$	2.50E-04	2.50E-04	3.67E-04
$Q_1(7)$	4.50E-04	3.50E-04	5.14E-04
$Q_1(8)$	4.50E-04	3.70E-04	5.14E-04
$Q_1(9)$	4.00E-04	5.20E-04	6.61E-04
$Q_1(10)$	6.50E-04	5.30E-04	6.61E-04
$Q_1(11)$	not observed	not observed	not observed
$Q_1(12)$	4.50E-04	5.60E-04	5.50E-04
$Q_2(6)$	1.00E-04	2.20E-04	2.20E-04
$Q_2(7)$	3.00E-04	2.50E-04	3.12E-04
$Q_2(8)$	4.50E-04	3.70E-04	4.77E-04
$Q_2(9)$	4.50E-04	3.90E-04	6.24E-04
$Q_2(10)$	6.50E-04	4.30E-04	5.87E-04
$Q_2(11)$	not observed	not observed	not observed
$Q_2(12)$	4.00E-04	6.00E-04	5.87E-04

the 2001 and 2004 data, the hypothesis of artefacts is reinforced. On the contrary, the MgH polarization peaks are common to both spectra and are not associated with any depression of the intensity, so that one can discard the idea that they are also artefacts. To confirm their reality, we have compared in Table 2 the polarization degrees determined in the 2001 and 2004 data with the polarization degrees determined in Gandorfer's atlas (Gandorfer 2000). All these polarization degrees, measured above the continuum, are in agreement, confirming thus the THEMIS results with the Gandorfer's results.

Strictly speaking, Gandorfer's results are in fact about 20% higher than THEMIS ones, especially in the Q_1 band (the agreement is much better inthe Q_2 band). This trend remains to be explained, but THEMIS 2001 and THEMIS 2004 differ also between themselves in the same order of magnitude, which has to be related to the polarimetric accuracy of the measurements, which is of a few 10^{-5}, as it can be seen in Bommier & Molodij (2002), Table 4, Cols. l (photon noise) and n (polarimetric noise when the true beam exchange is used as here), for the sodium D lines that are not so far in wavelength, and as it can be seen also in the continuum in Fig. 1. Another source of inaccuracy in the results is the definition of the continuum level: the difficulty and the ensuing inaccuracy, may be higher than the few 10^{-5}, can be appreciated in Fig. 1.

3. Recalculation of the Hönl-London factors

As different values can be found in the literature for the oscillator strengths of the lines under interest (Kurucz's values are reported in Table 1; Weck et al. 2003, derive twice smaller values), we have found necessary to recalculate the Hönl-London factors of these lines. This calculation is based on the most recent basic reference works in this field by Larsson (1983) and Whiting & Nicholls (1974). We adopt their definitions, and also the conventions of Brink & Satchler (1968).

We apply the Hund's case (b), which is valid for Σ states and for large j of Π states. Then, the rovibronic wavefunctions can be decomposed in a vibration part and a rotation part

$$|v\Lambda NS\,jm\rangle = \sum_{Mm_S}(-1)^{N+S-m} \times\sqrt{2j+1}\begin{pmatrix} N & S & j \\ M & m_S & -m\end{pmatrix}|NM\Lambda\rangle\,|v\Lambda S\,m_S\rangle\,, \quad (1)$$

where

$$|NM\Lambda\rangle = \sqrt{\frac{2N+1}{8\pi^2}}(-1)^{M-\Lambda}\left[\mathcal{D}^N_{M\Lambda}(\omega)\right]^* \quad (2)$$

is the rotational wave function.

The transitions take place between states of assigned parity (with a parity change in a dipole electric transition). For the given case of the $A^2\Pi$–$X^2\Sigma^+$ transition, these states are respectively

– for the lower state $\Lambda'' = 0$

$$\left|v''\ \Lambda''=0\ N''S''j''m''\right\rangle = \sum_{M''m_S}(-1)^{N''+S''-m''} \times\sqrt{2j''+1}\begin{pmatrix} N'' & S'' & j'' \\ M''m_{S''} & -m''\end{pmatrix} \times\left|N''M''\Lambda''\right\rangle\left|v''\ \Lambda''=0\ S''m_{S''}\right\rangle; \quad (3)$$

– for the upper state $\Lambda' = \pm 1$

$$\begin{aligned}\left|v'\ \Lambda' = \pm 1\ N'S'j'm'\right\rangle = &\sum_{M'm_S}(-1)^{N'+S'-m'}\\ &\times\sqrt{2j'+1}\begin{pmatrix}N' & S' & j'\\ M' & m_{S'} & -m'\end{pmatrix}\\ &\times\frac{1}{\sqrt{2}}\left[\left|N'M'\Lambda'\right\rangle\left|v'\Lambda'S'm_{S'}\right\rangle\right.\\ &\left.\pm\left|N'M'-\Lambda'\right\rangle\left|v'-\Lambda'S'm_{S'}\right\rangle\right].\end{aligned}\tag{4}$$

The dipole is defined as

$$\left[r_q\right]_{\rm SF} = \sum_\sigma [r_\sigma]_{\rm BF}\left[\mathcal{D}^1_{q\sigma}(\omega)\right]^*,\tag{5}$$

where $\mathcal{D}^1_{q\sigma}(\omega)$ is the rotation matrix of Euler angles ω from the space fixed (SF) reference frame of the laboratory, to the body fixed (BF) reference frame linked to the molecule. One uses the following definition of the dipole-length molecule operator

$$r_{q=\pm1} = \frac{x \pm {\rm i}y}{\sqrt{2}}.\tag{6}$$

The dipole matrix element is

$$\begin{aligned}D = &\left\langle v''\Lambda''N''S\,j''m''\right|r_q\left|v'\Lambda'N'S\,j'm'\right\rangle\\ = &\sum_{M'M''m_S}\sum_\sigma\frac{\sqrt{(2j'+1)(2j''+1)}}{\sqrt{2}}\\ &\times(-1)^{N'+N''+2S-m'-m''}\\ &\times\begin{pmatrix}N' & S & j'\\ M' & m_S & -m'\end{pmatrix}\begin{pmatrix}N'' & S & j''\\ M'' & m_S & -m''\end{pmatrix}\\ &\times\left[\left\langle v''\Lambda''Sm_S\right|r_\sigma\left|v'\Lambda'Sm_S\right\rangle\right.\\ &\times\left\langle N''M''\Lambda''\right|\left[\mathcal{D}^1_{q\sigma}\right]^*\left|N'M'\Lambda'\right\rangle\\ &\pm\left\langle v''\Lambda''Sm_S\right|r_\sigma\left|v'-\Lambda'Sm_S\right\rangle\\ &\left.\times\left\langle N''M''\Lambda''\right|\left[\mathcal{D}^1_{q\sigma}\right]^*\left|N'M'-\Lambda'\right\rangle\right],\end{aligned}\tag{7}$$

where $S' = S'' = S$ is unaffected by r_q. The angular integral can then be reduced as

$$\begin{aligned}\left\langle N''M''\Lambda''\right|\left[\mathcal{D}^1_{q\sigma}\right]^*\left|N'M'\Lambda'\right\rangle = &\sqrt{(2N'+1)(2N''+1)}(-1)^{M''+q-\sigma}\\ &\times\begin{pmatrix}N'' & 1 & N'\\ M''-q & q & -M'\end{pmatrix}\begin{pmatrix}N'' & 1 & N'\\ \Lambda''-\sigma & -\sigma & -\Lambda'\end{pmatrix},\end{aligned}\tag{8}$$

so that the dipole matrix element can be reduced as

$$\begin{aligned}D = &\frac{\sqrt{(2j'+1)(2j''+1)(2N'+1)(2N''+1)}}{\sqrt{2}}\\ &\times(-1)^{S-m'+\sigma}\\ &\times\begin{Bmatrix}j' & N' & S\\ N'' & j'' & 1\end{Bmatrix}\\ &\times\begin{pmatrix}j' & j'' & 1\\ m' & -m'' & q\end{pmatrix}\begin{pmatrix}N'' & 1 & N'\\ \Lambda'' & -\sigma & -\Lambda'\end{pmatrix}\\ &\times\left[\left\langle v''\Lambda''S\right|r_\sigma\left|v'\Lambda'S\right\rangle \pm \left\langle v''\Lambda''S\right|r_{-\sigma}\left|v'-\Lambda'S\right\rangle\right].\end{aligned}\tag{9}$$

In this expression, the two vibrational matrix elements are equal because $\Lambda'' = 0$.

The line strength can be computed as

$$\begin{aligned}S(v''j''\Lambda'', v'j'\Lambda') = &\sum_{m'm''q}|D|^2\\ = &\,2(2j'+1)(2j''+1)(2N'+1)(2N''+1)\\ &\times\begin{Bmatrix}j' & N'S\\ N'' & j''\,1\end{Bmatrix}^2\begin{pmatrix}N''1N'\\ 0\ \ 1{-}1\end{pmatrix}^2\\ &\times\left|\left\langle v''\Lambda''S\right|r_\sigma\left|v'\Lambda'S\right\rangle\right|^2.\end{aligned}\tag{10}$$

Introducing

$$d^2 = \left|\left\langle v''\Lambda''S\right|r_\sigma\left|v'\Lambda'S\right\rangle\right|^2\tag{11}$$

and writing

$$S(v''j''\Lambda'', v'j'\Lambda') = S_{j'j''} = d^2\mathcal{S}_{j'j''},\tag{12}$$

where $\mathcal{S}_{j'j''}$ is the line Hönl-London factor, one can derive these factors for each line of the $A^2\Pi$–$X^2\Sigma^+$ transition

$$\begin{cases}Q_1\ \mathcal{S}_{j'j''} = \frac{(2j'-1)(j'+1)}{j'} = \frac{(2j''-1)(j''+1)}{j''}\\ Q_2\ \mathcal{S}_{j'j''} = \frac{j'(2j'+3)}{j'+1} = \frac{j''(2j''+3)}{j''+1}\\ P_1\ \mathcal{S}_{j'j''} = \frac{(2j'-1)(2j'+3)}{4(j'+1)} = \frac{(2j''-3)(2j''+1)}{4j''}\\ P_2\ \mathcal{S}_{j'j''} = \frac{(2j'+1)^2}{4(j'+1)} = \frac{(2j''-1)^2}{4j''}\\ R_1\ \mathcal{S}_{j'j''} = \frac{(2j'+1)^2}{4j'} = \frac{(2j''+3)^2}{4(j''+1)}\\ R_2\ \mathcal{S}_{j'j''} = \frac{(2j'-1)(2j'+3)}{4j'} = \frac{(2j''+1)(2j''+5)}{4(j''+1)}\end{cases},\tag{13}$$

where

$$\begin{cases}Q_1\ N''=N' & j'=N'+\frac12\ j''=N''+\frac12\\ Q_2\ N''=N' & j'=N'-\frac12\ j''=N''-\frac12\\ P_1\ N''=N'+1 & j'=N'+\frac12\ j''=N''+\frac12\\ P_2\ N''=N'+1 & j'=N'-\frac12\ j''=N''-\frac12\\ R_1\ N''=N'-1 & j'=N'+\frac12\ j''=N''+\frac12\\ R_2\ N''=N'-1 & j'=N'-\frac12\ j''=N''-\frac12\end{cases}.\tag{14}$$

The resulting sum rule is

$$\begin{aligned}\sum_{j'',\Delta j=\Delta N}\mathcal{S}_{j'j''} = &\sum_{j',\Delta j=\Delta N}\mathcal{S}_{j'j''}\\ = &\,4(2j+1) - \frac{3(2j+1)}{2j(j+1)},\end{aligned}\tag{15}$$

where j stands for j' or j''. This sum rule includes only the 6 lines listed in Eq. (14), which are the principal ones and which obey $\Delta j = \Delta N$. However, secondary weaker lines exist having $\Delta j \neq \Delta N$. When these lines are also taken into account, the sum rule becomes

$$\sum_{j''}\mathcal{S}_{j'j''} = \sum_{j'}\mathcal{S}_{j'j''} = 4(2j+1),\tag{16}$$

that can be derived directly from Eq. (10), and that is in agreement with Larsson (1983) and Whiting & Nicholls (1974) for the present case where $S = 1/2$. Both sum rules coincide at the limit of large j.

From Larsson (1983), the Einstein spontaneous emission probability for one component is

$$A_{v'j',v''j''} = \frac{64\pi^4 e^2 a_0^2}{3h}\nu^3 d^2 \frac{\mathcal{S}_{j'j''}}{2j'+1}, \tag{17}$$

and the band spontaneous emission probability is

$$A_{v'v''} = \frac{64\pi^4 e^2 a_0^2}{3h}\bar{\nu}^3 d^2 \frac{2-\delta_{0,\Lambda'+\Lambda''}}{2-\delta_{0,\Lambda'}}, \tag{18}$$

so that

$$A_{v'j',v''j''} = A_{v'v''}\frac{2-\delta_{0,\Lambda'}}{2-\delta_{0,\Lambda'+\Lambda''}}\ \frac{\mathcal{S}_{j'j''}}{2j'+1}. \tag{19}$$

And as for the oscillator strength, one has for each component

$$f_{v'j',v''j''} = \frac{8\pi^2 mca_0^2}{3h}\nu d^2 \frac{\mathcal{S}_{j'j''}}{2j''+1}, \tag{20}$$

and, for the band

$$f_{v'v''} = \frac{8\pi^2 mca_0^2}{3h}\bar{\nu} d^2 \frac{2-\delta_{0,\Lambda'+\Lambda''}}{2-\delta_{0,\Lambda''}}, \tag{21}$$

leading to

$$f_{v'j',v''j''} = f_{v'v''}\frac{2-\delta_{0,\Lambda''}}{2-\delta_{0,\Lambda'+\Lambda''}}\ \frac{\mathcal{S}_{j'j''}}{2j''+1}. \tag{22}$$

In the case of the Q_1 and Q_2 lines of MgH, this leads to $f_{v'j',v''j''} = f_{v'v''}/2$ at the large j limit, whereas the similar formulae (3) and (4) of Weck et al. (2003) lead to $f_{v'j',v''j''} = f_{v'v''}/4$. Moreover, using formulae (3) and (4) of Weck et al. (2003) leads to $f_{v'v''}/2$ instead of $f_{v'v''}$ when the band oscillator strength $f_{v'v''}$ is recalculated from the elementary oscillator strengths $f_{v'j',v''j''}$. The Hönl-London factors of Weck et al. (2003) do not agree with the ones of our Eq. (13), because we found that Weck et al. (2003) did their calculation assuming $S = 0$, dividing the line strengths by 2 at the end of the calculation to take into account the fact that the spin is not 0 but 1/2. The result is that their sum rule (normalization condition) is not the same as ours, which is also in agreement with Larsson (1983) and Whiting & Nicholls (1974). For the ($v' = v'' = 0$) band, Weck et al. (2003) computed the band oscillator strength $f_{v'v''} = 0.1616$, which leads to $f_{v'j',v''j''} \approx 0.08$ for the Q-band following Eq. (22) (in the large j limit). This value is in agreement with the Kurucz's values reported in Table 1 and used in the present work. The detailed values $f_{v'j',v''j''} \approx 0.04$ obtained by applysing their formulae (3) and (4) and provided on the web for the Q-band by Weck et al. (2003) are too small by a factor 2.

4. Interpretation

4.1. First step: the differential Hanle effect in zero depolarizing collision rate

According to the theory of the differential Hanle effect, the ratio of polarization of two weak molecular lines of the same band (having nearly same lower level population, depolarizing collision rates and radiative rates) is given by the expression:

$$R_{\rm pol} = \frac{Q/I}{Q'/I'} = \frac{g_{\rm deg}}{g'_{\rm deg}}\frac{W_{\rm H}}{W'_{\rm H}}\frac{W_2}{W'_2}\frac{W_{\rm c}}{W'_{\rm c}}, \tag{23}$$

where

- $g_{\rm deg}$ is the upper level degeneracy

$$\begin{cases} g_{\rm deg} = 2N_\ell + 2 & (Q_1 \text{ band}) \\ g_{\rm deg} = 2N_\ell & (Q_2 \text{ band}) \end{cases}; \tag{24}$$

- $W_{\rm H}$ is the Hanle depolarization parameter, that is for a turbulent field (Stenflo 1982)

$$W_{\rm H} = 1 - \frac{2}{5}\left[\frac{\Gamma_{\rm H}^2}{1+\Gamma_{\rm H}^2} + \frac{4\Gamma_{\rm H}^2}{1+4\Gamma_{\rm H}^2}\right], \tag{25}$$

  where the Hanle parameter $\Gamma_{\rm H}$ depends on the upper level Landé factor $g_{J'}$, on the magnetic field B and on the upper level alignment inverse lifetime

$$\Gamma_{\rm H} = 0.88\frac{g_{J'}B}{\gamma_{\rm R}+\gamma_{\rm I}+D^{(2)}}, \tag{26}$$

  the field strength B being expressed in Gauss and the rates in the denominator in units of 10^7 s^{-1}. The Landé factors $g_{J'}$, which are given in the last column of Table 1, have been computed by assuming Hund's case (b). The upper level alignment inverse lifetime involves three contributions: the radiative inverse lifetime $\gamma_{\rm R}$, the inelastic collisional inverse lifetime $\gamma_{\rm I}$ that is negligible with respect to $\gamma_{\rm R}$ in the solar atmosphere, and the elastic collisional depolarizing rate $D^{(2)}$. Neglecting $\gamma_{\rm I}$, Eq. (26) is nothing else than Eq. (7) of Berdyugina & Fluri (2004), also Eq. (5) of Faurobert & Arnaud (2003), and also Eq. (6) of Trujillo Bueno (2003a). As the lines under interest belong to the same band, $\Gamma_{\rm H}/g_{J'}$ isnearly the same for all the lines, which permits to compute the ratio $W_{\rm H}/W'_{\rm H}$ as a function of it;
- W_2 is the line polarizability. Analytical values of this coefficient have been provided by Landi Degl'Innocenti (2003), for the present MgH transition, leading to the numerical values reported in the last column of Table 1;
- $W_{\rm c}$ is the collisional depolarizing factor

$$W_{\rm c} = \frac{\gamma_{\rm R}}{\gamma_{\rm R}+\gamma_{\rm I}+D^{(2)}}. \tag{27}$$

  However, in the following we neglect the departure from unity of $W_{\rm c}/W'_{\rm c}$, by considering that the quantum numbers ofall the lines over interest are not highly different one from each other, which should lead to not very different rates (similarly to the W_2 coefficients listed in Table 1). In this respect, it could be argued that is not completely correct to derive line by line depolarizing rates as we do below in the second step. However, as these final rates are found very close one from each other (see Table 3), the procedure is finally justified;
- the level population differences (and the Boltzmann factor differences), and the radiative rate and profile differences, are neglected in this equation, that is then true only for neighboring lines belonging to the same band (for the general case, see for instance Eq. (1) and the related discussion in Berdyugina & Fluri 2004).

$W_{\rm H}/W'_{\rm H}$ is unity for zero field and also for infinitely large field. In between, two possible values of $\Gamma_{\rm H}/g_{J'}$ can then account for a given value of $R_{\rm pol}$. More different are the lines parameters, more sensitive is the $\Gamma_{\rm H}$ determination. In this respect, we have analyzed the ratios $Q_1(6)/Q_1(12)$ and $Q_2(6)/Q_2(12)$ of the THEMIS 2004 data. THEMIS 2004 data have been retained preferably to THEMIS 2001 and Gandorfer's atlas data, because

Table 3. Interpretation of the observed polarization (THEMIS 21 November 2004 data). The maximum polarization is a result of computation, assuming neither collisional nor magnetic depolarization. The molecular lines being absent of the intensity spectrum, the height is the continuum formation height. The polarization formation height is of the order of 200 km (see text and Fig. 4).

(N_ℓ)	Observed polarization	Maximum polarization	Height km	Γ_H	$\alpha^{(2)}$ $cm^3\ s^{-1}$	$D^{(2)}$ at h = 200 km s^{-1}	B at h = 200 km Gauss
$Q_1(6)$	2.50E-04	1.33E-03	169.13	0.73	1.20E-09	4.18E+07	28.85
$Q_1(7)$	3.50E-04	1.49E-03	169.94	0.62	9.76E-10	3.42E+07	25.16
$Q_1(8)$	3.70E-04	1.64E-03	170.77	0.53	1.20E-09	4.20E+07	28.72
$Q_1(9)$	5.20E-04	1.79E-03	172.47	0.47	8.70E-10	3.04E+07	23.30
$Q_1(10)$	5.30E-04	1.93E-03	175.79	0.42	1.05E-09	3.69E+07	26.26
$Q_1(11)$	not observed	1.99E-03	172.41	0.38			
$Q_1(12)$	5.60E-04	2.07E-03	172.80	0.35	1.18E-09	4.13E+07	28.20
$Q_2(6)$	2.20E-04	1.13E-03	168.06	0.54	1.43E-09	5.02E+08	33.03
$Q_2(7)$	2.50E-04	1.30E-03	168.94	0.47	1.62E-09	5.69E+08	35.94
$Q_2(8)$	3.70E-04	1.46E-03	169.81	0.42	1.16E-09	4.07E+07	28.22
$Q_2(9)$	3.90E-04	1.61E-03	171.55	0.38	1.32E-09	4.63E+07	30.76
$Q_2(10)$	4.30E-04	1.76E-03	174.96	0.35	1.39E-09	4.85E+07	31.70
$Q_2(11)$	not observed	1.83E-03	171.58	0.32			
$Q_2(12)$	6.00E-04	1.92E-03	172.00	0.30	9.95E-10	3.48E+07	25.26
average			**171.44**		**1.20E-09**	**4.20E+07**	**28.78**
±st.dev.					**±0.21E-09**	**±0.72E+07**	**±3.47**

$Q_2(6)$ differs not too much from $Q_1(6)$, and also because in these data the polarization degrees increase when going from $N = 6$ to $N = 12$, following thus the theoretical behavior (see the theoretical maximum polarization behavior in Table 3), whereas in the 2001 and Gandorfer's atlas data the polarization degrees decrease in the high N side, contrarily to the theoretical behavior. Retaining the lower value of $\Gamma_H/g_{J'}$, that corresponds to the lower magnetic field value, we derive from these two pairs of THEMIS 2004 lines

$$\Gamma_H/g_{J'} = 4.05 \pm 1.75, \tag{28}$$

where the second number accounts for the standard deviation. In order to apply then Eq. (26) to the field strength derivation, one is faced with the problem that the $D^{(2)}$ relaxation rates are presently completely unknown for MgH. So $D^{(2)} = 0$ is usually assumed. Under this hypothesis, we thus derive from the values of $\Gamma_H/g_{J'}$ given above the preliminary field strength

$$B_{\rm pre\,lim} = 9.2 \pm 4.0 \text{ Gauss}, \tag{29}$$

in agreement with the value of 7 Gauss derived by the other authors.

4.2. Second step: derivation of the depolarizing collision rate froma radiative transfer model

The next step is to enter this result in a model of NLTE line polarization formation, where the two depolarizing mechanisms compete: the elastic collisional depolarization and the magnetic Hanle depolarization (expressed in terms of the above Γ_H parameter). As Γ_H has now been fixed, only one free parameter remains, $D^{(2)}$, that can be derived by comparing the computed polarization to the observed one.

We have used a generalization to these MgH lines of the model used by Bommier et al. (2005) for computing the Sr I 4607 Å line second solar spectrum. This model is based on the density matrix theory of the polarized raditive transfer for a 2-level atom imbedded in aweak magnetic field (Hanle effect) developed by Landi Degl'Innocenti et al. (1990).

In a first step, the question arises of the validity of the 2-level approximation for describing the $Q_{1,2}(6–12)$ MgH lines. Figure 3 of Landi Degl'Innocenti (2003) shows that every upper level of this band is pumped by only one lower level, so that the approximation applies. In other words, each upper level of the MgH Q-band is connected with only one lower level, so that the upper level inverse life-time coincides with the Einstein coefficient for spontaneous emission in this transition (other transitions are neglected because of lower oscillator strengths).

The largest difference with the method used for Sr I 4607 lies in the determination of the line opacity with respect to the continuum opacity. In this determination, which implies now the introduction of the dissociation equilibrium for computing the MgH lower level population. In this purpose, we have used the value 1.34 eV for the dissociation potential (instead ofthe Herzberg's 2.0 eV value). The lower level excitation potentials listed in Table 1 have been derived from the Herzberg rotational constant $B_v = 5.735\ cm^{-1}$ by

$$E_{\rm exc.pot.} = B_v N_\ell (N_\ell + 1). \tag{30}$$

The Mg abundance has been taken as 7.58, in the usual logarithmic scale where the abundance of hydrogen is 12. The partition functions are from Wittmann.

The atmosphere model is the same as in Bommier et al. (2005), and is displayed in Fig. 2. The micro- and macroturbulent velocities are taken into account in the same way as in that paper, and in the present analysis we have introduced the $v_{\rm micro}$ and $v_{\rm macro}$ values there derived, namely

$$v_{\rm micro} = 1.87\ km\ s^{-1},$$
$$v_{\rm macro} = 1.78\ km\ s^{-1}. \tag{31}$$

The height of line center formation is derived by applying the Eddington-Barbier approximation, where the optical depth includes both line and continuum contribution. As the line optical depth is small, this depthis mainly the one of the continuum. The obtained list of depths is given in Table 3. The collisional deexcitation coefficient ε', which is unknown also, has been taken to be 10^{-4}, which is a typical value instellar atmospheres. In fact, using this value leads to a negligible effectof this coefficient on the line polarization. Taking $\varepsilon' = 10^{-2}$ would lead to a polarization degree decrease of 2×10^{-6}, which is lower than the polarization inaccuracy. The polarization accuracy level would be reached with $\varepsilon' = 10^{-1}$, which leads to a polarization degree decrease of 3×10^{-5}. However this sensitive value, $\varepsilon' = 10^{-1}$, is improbable in stellar atmospheres, so that the effect of ε' can be neglected.

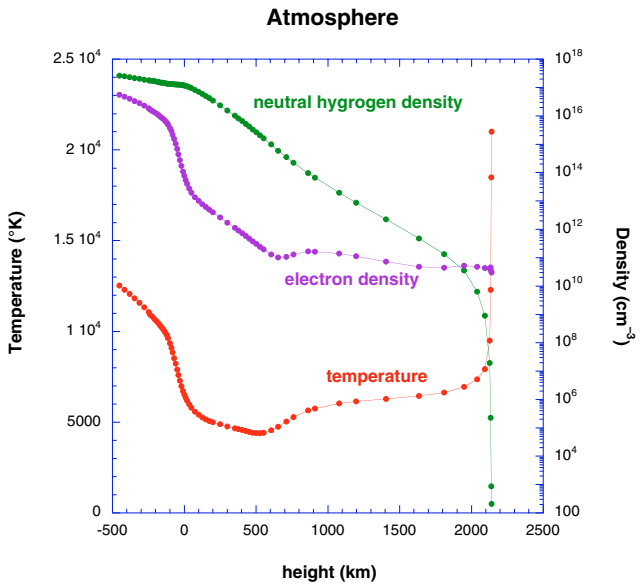

Fig. 2. Atmosphere model: Maltby et al. Quiet Sun Photospheric Reference Model (Maltby et al. 1986), extrapolated downwards beyond −70 km to −450 km below the $\tau_{5000} = 1$ level. Above −70 km, this model is very similar to the Quiet Sun FAL C (Fontenla et al. 1993).

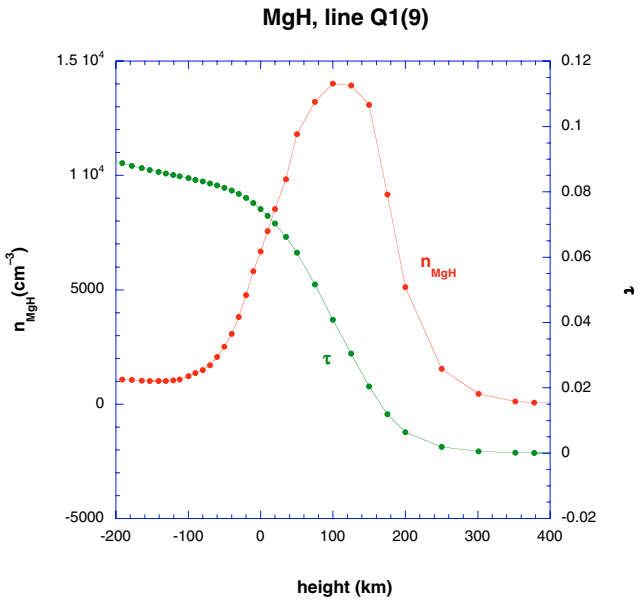

Fig. 3. Lower level population of the $Q_1(9)$ line of the $A^2\Pi-X^2\Sigma^+$ (0. 0) MgH transition, as a function of height above the $\tau_{5000} = 1$ level. The $Q_1(9)$ line optical depth is also displayed.

The Einstein coefficients provided in Table 1 have been derived from the gf values given in the Kurucz's data base. These values are in excellent agreement with the value $f^{\rm abs}_{J'J''} = 0.0808$ for the lines of the $v' = v'' = 0$ Q-band that can be derived from Weck et al. (2003).

Table 3 displays also the polarization computed in the absence of both depolarizing mechanisms, namely elastic collisions and magneticfield, as the "maximum polarization".

As a result of our model, Fig. 3 displays the variation with depth in the atmosphere, of the lower level population of one of the lines, and also of the line optical depth. Though the lower level population is maximum around $h = 100$ km, the line polarization is formed upper, as it results from the contribution functions for the Stokes parameter Q that are plotted in Fig. 4. It results from these contribution functions that the polarization is formed at $h = 200 \pm 80$ km, which is higher than the continuum formation height displayed in Table 3 as it has to be expected. The contribution function that we have plotted is the contribution of each depth interval to the integral (see for instance the contribution of each interval in Eq. (27) of Bommier et al. 1991). As it can be seen along the temperature curve, the depth points are not exactly equally spaced, so that the plotted contribution functions are rough, but sufficient for the present analysis.

The method for determining the $D^{(2)}$ rates is as follows: first, the value of $\Gamma_{\rm H}$ for each line is derived from the above $\Gamma_{\rm H}/g_{J'}$ line-independent value. This value is entered in the code as input data, and the free depolarizing rate per colliding hydrogen atom $\alpha^{(2)}$ is determined by adjusting the computed polarization to the observed one, with

$$D^{(2)} = N_{\rm H}\alpha^{(2)}, \tag{32}$$

$N_{\rm H}$ being taken from the atmosphere model. The obtained values are given in Table 3, and are found rather constant among the different lines. We then derive the average value

$$\bar{\alpha}^{(2)} = (1.20 \pm 0.21) \times 10^{-9}\ {\rm cm}^3\ {\rm s}^{-1}, \tag{33}$$

0.21 being the standard deviation.

4.3. Third step: taking into account the depolarizing collision rate in the Hanle effect

Finally, the final magnetic field strength $B_{\rm final}$ is derived from Eq. (26), neglecting $\gamma_{\rm I}$ and taking into account the $D^{(2)}$ values derived from Eq. (32) applied to the above determined $\alpha^{(2)}$ elementary rates, at $h = 200$ km where the polarization is formed (see Fig. 4), where the hydrogen density taken from the model is 3.5×10^{16} cm^{-3}. The results and the field strengths are listed in Table 3, whose average values are

$$\bar{D}^{(2)} = (4.2 \pm 0.7) \times 10^7\ {\rm s}^{-1}, \tag{34}$$

$$\bar{B}_{\rm final} = 29 \pm 12\ {\rm Gauss}. \tag{35}$$

3.5 Gauss is the standard deviation through the lines, and coincides, as expected, with the inaccuracy on $\bar{B}_{\rm final}$ resulting from the standard deviation of the above determined $\bar{\alpha}^{(2)}$ rate. However, one has also to take into account the 40% inaccuracy on the $\Gamma_{\rm H}$ determination (see Eqs. (28)–(29)), which leads to the present final 12 Gauss uncertainty.

5. Conclusion

Figure 5 displays the value of $\bar{B}_{\rm final}$ determined above in Eq. (35). The vertical error bar results from the 40% inaccuracy of the differential Hanle effect method applied to such weakly polarized and similar lines. The associated height value is the one of the contribution function maximum as it can be seen in Fig. 4. The horizontal error bar was determined from the function width. On this figure, we have also reported the Sr I 4607 Å results of Bommier et al. (2005), the horizontal error bars being also derived from the Sr I 4607 Å Stokes Q contribution function. The conclusion is as follows: when the depolarizing collisions are taken into account, the field value determined with the MgH lines (29 ± 12 Gauss) becomes much closer to the one determined with Sr I 4607 Å (46 Gauss), contrarily to what previously determined when ignoring the collisional depolarization effect. Thus, given the error bars, it appears no more necessary to

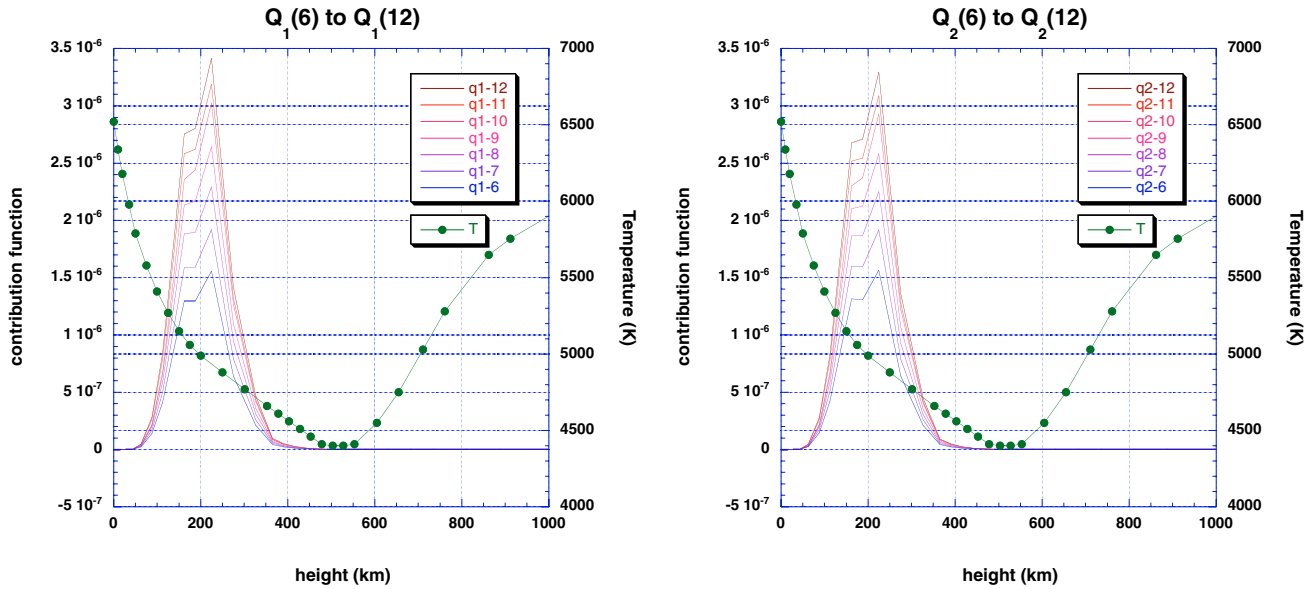

Fig. 4. Contribution functions for the emerging polarization (Stokes Q) of the MgH lines (in Y1), and temperature (in Y2), as a function of the height above $\tau_{5000} = 1$.

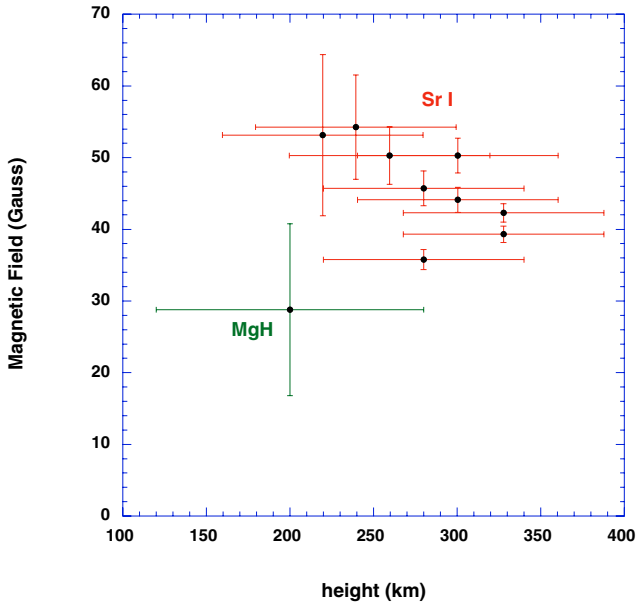

Fig. 5. Values of the turbulent magnetic field strength as a function of the height above $\tau_{5000} = 1$, determined from the Sr I 4607 Å line limb polarization by Bommier et al. (2005) and from the MgH lines analyzed in the present paper.

put forward different formation regions for MgH and Sr I lines, as done for C_2 and Sr I by Trujillo Bueno et al (2004), where the depolarizing effect of collisions was not taken into account.

Finally, our present method can be found rather complicate and evenincoherent, because Γ_H, which is determined at the first step, is taken height-independent, where as $D^{(2)}$, which is determined at the third step, is height-dependent there, and it can be remarked that Γ_H depends in fact on $D^{(2)}$, as it can be seen from Eq. (26). The present analysis has surely to be redone by jointly determining Γ_H and $D^{(2)}$ from the results of the transfer code run for each line of the series. However, we do not expect highly different results.

At the end of this work, we have to compare our results with the recent ones by Asensio Ramos & Trujillo Bueno (2005), who have analyzed the same MgH lines included in a larger sample (extending up to $N_\ell = 37$) measured in Gandorfer's Atlas (Gandorfer 2000), and who have applied a 3D radiative transfer model for computing the MgH abundance (the radiative transfer model for computing the emerging polarization is unfortunately poorly described in that paper). It has to be emphasized that for $N_\ell > 12$, the second solar spectrum is much more complex and the lines may be blended and become hardly distinguishable. Asensio Ramos & Trujillo Bueno conclude to a higher depolarizing collisional rate, $\delta_u = D^{(2)}/A \simeq 9$, and to a lower field strength, $B < 10$ Gauss, whereas we obtain a more than four times lower depolarizing collisional rate $\delta_u = D^{(2)}/A \simeq 2$ at $h = 200 \pm 80$ km where the polarization is formed (see Table 3), associated to the higher field strength $B = 29 \pm 12$ Gauss. It has to be emphasized that this $D^{(2)}$ depolarizing collisional rate (and the reduced rate δ_u) depends linearly on the neutral Hydrogen density N_H. That is the reason why we have determined, not $D^{(2)}$, but the rate per colliding hydrogen atom $\alpha^{(2)} = D^{(2)}/N_H$, which is model-independent, and we have then derived $D^{(2)}$ at the height of polarization formation. Asensio Ramos & Trujillo Bueno do not seem to have explicitly taken into account this model dependence of δ_u. It has to be remarked that Asensio Ramos & Trujillo Bueno (2005) use Einstein coefficients twice lower than ours (see their Sect. 3), because derived from Weck et al. (2003) who give twice too small oscillator strengths (see our Sect. 3). This modifies only the final magnetic field value (reducing it by a factor two), but not the solution of the radiative transfer equations that are expressed in reduced quantities, all scaled by the Einstein coefficient A: thus, if Asensio Ramos & Trujillo Bueno use the true oscillator strengths as given in our Table 1, they would derive a twice larger magnetic field, $B < 20$ Gauss, which does not disagree with our value $B = 29 \pm 12$ Gauss, and which is nearly compatible with the value derived from the Sr I 4607 Å line polarization (46 Gauss). Again, it is then unnecessary to invoke different formation regions for Sr I and MgH.

Another result has to be mentioned: Mohan Rao & Rangarajan (1999) have interpreted the polarization observed by Stenflo & Keller (1997) in two other MgH lines of the same

band. As us, they have used a plane-parallel model of polarized radiative transfer. By comparing the observed profile to the theoretical one, they determined three parameters for each line: the radiative de-excitation coefficient, the collisional de-excitation coefficient and the depolarizing collision rate. Their depolarizing collision rates are smaller, for one line, or of the same order of magnitude as ours, for the other line. They have not introduced any magnetic depolarization: at that time (1999) it was generally believed that the molecules were "immune to the Hanle effect". If, as we do, a magnetic depolarization was introduced, even lower depolarizing collision rates would be derived. It has however to be noticed that the de-excitation coefficients derived by these authors give $\varepsilon' > 0.5$, which is improbable in stellar atmosphere and contributes to depolarize the lines.

In any case, the present knowledge of the MgH excited state collisional rates is too weak to discriminate between these different results.

Acknowledgements. The authors are indebted to A. Asensio Ramos for fruit ful discussions and having kindly provided molecular data. We thank a lot the anonymous referee of this paper for a very helpful critical reading of the manuscript.

References

Arnaud, J., Mein, P., & Rayrole, J. 1998, Proceedings of A Crossroads for European Solar & Heliospheric Physics, Tenerife, 1998 March 23–27, ESA SP-417, 213
Asensio Ramos, A., & Trujillo Bueno, J. 2005, ApJ, 635, L109
Berdyugina, S. V., & Fluri, D. M. 2004, A&A, 417, 775
Berdyugina, S. V., Stenflo, J. O., & Gandorfer, A. 2002, A&A, 388, 1062
Bommier, V., & Molodij, G. 2002, A&A, 381, 241
Bommier, V., & Rayrole, J. 2002, A&A, 381, 227
Bommier, V., Leroy, J. L., & Sahal-Bréchot, S. 1981, A&A, 100, 231
Bommier, V., Landi Degl'Innocenti, E., & Sahal-Bréchot, S. 1991, A&A, 244, 383
Bommier, V., Derouich, M., Landi Degl'Innocenti, E., Molodij, G., & Sahal-Bréchot, S. 2005, A&A, 432, 295
Brink, D. M., & Satchler, G. R. 1968, Angular Momentum (Oxford: Clarendon Press)
Faurobert, M., & Arnaud, J. 2002, A&A, 382, L17
Faurobert, M., & Arnaud, J. 2003, A&A, 412, 555
Faurobert, M., Arnaud, J., Vigneau, J., & Frisch, H. 2001, A&A, 378, 627
Fontenla, J. M., Avrett, E. H., & Loeser, R. 1993, ApJ, 406, 319
Gandorfer, A. 2000, The Second Solar Spectrum. A high spectral resolution polarimetric survey of scattering polarization at the solar limb in graphical representation. Volume I: 4625 Å to 6995 Å. Hochschulverlag AG an der ETH Zürich
Landi Degl'Innocenti, E. 1982, Sol. Phys., 79, 291
Landi Degl'Innocenti, E. 2003, in Solar Polarization 3, ed. J. Trujillo Bueno, & J. Sánchez Almeida, ASP Conf. Ser., 307, 164
Landi Degl'Innocenti, E., Bommier, V., & Sahal-Bréchot, S. 1990, A&A, 235, 459
Larsson, M. 1983, A&A, 128, 291
Maltby, P., Avrett, E. H., Carlsson, M., et al. 1986, ApJ, 306, 284
Mohan Rao, D., & Rangarajan, K. E. 1999, ApJ, 524, L139
Schadee, A. 1964, Bull. Astr. Inst. of the Netherlands, 17, 311
Stenflo, J. O. 1982, Sol. Phys. 80, 209
Stenflo, J. O., & Keller, C. U. 1997, A&A, 321, 927
Trujillo Bueno, J. 2003a, in Modelling of Stellar Atmospheres, ed. N. Piskunov, W. W. Weiss, & D. F. Gray (Kluwer), IAU Symp., 210
Trujillo Bueno, J. 2003b, in Solar Polarization 3, ed. J. Trujillo Bueno, & J. Sánchez Almeida, ASP Conf. Ser., 307, 407
Trujillo Bueno, J., Shchukina, N., & Asensio Ramos, A. 2004, Nature, 430, 326
Weck, P. F., Schweitzer, A., Stancil, P. C., &Hauschildt, P. H. 2003, ApJ, 582, 1059
Whiting, E. E., & Nicholls, R. W. 1974, ApJS, 27, 1